

Polarization discontinuity induced two-dimensional electron gas at ZnO/Zn(Mg)O interfaces: A first-principles study

J. Betancourt,¹ J. J. Saavedra-Arias,² J. D. Burton,³ Y. Ishikawa,² E. Y. Tsybmal,³ and J. P. Velev^{1,3}

¹*Department of Physics, Institute of Functional Nanomaterials, University of Puerto Rico, San Juan, Puerto Rico 00931, USA*

²*Department of Chemistry, Institute of Functional Nanomaterials, University of Puerto Rico, San Juan, Puerto Rico 00931, USA*

³*Department of Physics and Astronomy, Nebraska Center for Materials and Nanoscience, University of Nebraska, Lincoln, Nebraska 68588, USA*

(Received 25 March 2013; revised manuscript received 24 June 2013; published 14 August 2013)

The discovery of a high-mobility two-dimensional electron gas (2DEG) in wurtzite ZnO/Zn(Mg)O heterostructures is promising for applications due to the high mobility of the carriers. In this paper, we study the formation and properties of the 2DEG at ZnO/Zn(Mg)O interfaces using first-principles calculations based on hybrid density functional theory. The 2DEG arises from the polarization discontinuity at the interface between the two materials. The uncompensated bound charge at the interface gives rise to an electric field in the bulk of ZnO which confines free carriers close to the interface. We find that the type of the confined carriers is determined by the interface termination, while the amount of charge and the confinement width could be controlled by the Mg doping and the device dimensions.

DOI: [10.1103/PhysRevB.88.085418](https://doi.org/10.1103/PhysRevB.88.085418)

PACS number(s): 73.20.-r, 71.28.+d, 73.21.Cd, 73.40.Gk

I. INTRODUCTION

The ability to grow atomically abrupt oxide interfaces has enabled the new field of oxide electronics.^{1–5} A fundamental development resulting from this ability is the discovery of a two-dimensional electron gas (2DEG) at oxide interfaces.^{6–19} In the original system, consisting of the nonmagnetic insulators LaMO₃ ($M = \text{Al, Ti}$) and SrTiO₃, and in similar systems, the polar interface causes a diverging electric potential which leads to electron reconstruction at the interface.⁹ This mechanism, however, leaves little freedom to tune the carrier concentration or the confinement width. Moreover, carrier mobilities at the LaMO₃/SrTiO₃ interfaces are low due to the high effective mass of the localized d bands. High-electron mobility transistor (HEMT) applications require a high degree of control of the carrier concentration and mobilities comparable to the semiconductor analogs. Spin-polarized 2DEGs have also been proposed for systems such as LaMnO₃/SrMnO₃,²⁰ GaTiO₃/SrTiO₃,²¹ LaAlO₃/EuO,²² or LaAlO₃/FeS₂.²³

Recently, a different type of system supporting a 2DEG, wurtzite ZnO/Zn(Mg)O heterostructures, has been investigated experimentally.^{24–32} These heterostructures are usually grown using molecular beam epitaxy;^{24,25} however, a 2DEG was also demonstrated in samples grown with metal-organic vapor deposition which is suitable for mass production.^{30,31} The presence of the 2DEG is normally confirmed by Hall effect and capacitance measurements.^{24,27,28} The observation of the quantum Hall effect²⁵ and the fractional quantum Hall effect²⁹ in these heterostructures testifies to the high quality of these interfaces. Charge concentrations on the order of 10^{13} cm^{-2} and extremely high mobilities exceeding $10^5 \text{ cm}^2 \text{ V}^{-1} \text{ s}^{-1}$ at low temperature have been demonstrated.^{26,28,29} Recently, a spin-polarized 2DEG at ZnO/Zn(Mg)O interfaces has been reported.^{31,32} The ferromagnetism was presumed to be carrier mediated and originating from the formation of Zn vacancies.

The ZnO/Zn(Mg)O system is not only interesting from a fundamental point of view, but also it could be suitable for electronic and spintronic applications. ZnO is a versatile semiconducting oxide with remarkable properties which already finds applications in electronics and optoelectronics. It

has a wide band gap of 3.4 eV, which can be tuned by doping with Mg or Cd,³³ making it a transparent material active in the ultraviolet (UV) region of the spectrum with applications in optoelectronics. Carriers have high mobility because they reside in the Zn- s band (Zn $3d^{10}$), making it suitable for HEMT applications.²⁶ In addition, ZnO was predicted to be a room temperature dilute magnetic semiconductor (DMS).³⁴ These considerations indicate that the ZnO/Zn(Mg)O system could potentially support a high-mobility spin-polarized 2DEG at room temperature.

First-principles calculations of the 2DEG at ZnO/Zn(Mg)O interfaces are lacking due to the deficiency of density functional theory (DFT) in predicting the band gap of semiconductors. These interfaces are quite different from the polar interfaces, such as LaAlO₃/SrTiO₃, which have been exhaustively studied. The consensus for the formation of the 2DEG is derived by analogy with modulation-doped III-V semiconductors (e.g. GaAs/AlAs, GaN/AlN). Like these materials, ZnO possesses spontaneous polarization in the bulk. The spontaneous polarization on both sides of the interface is different due to the different atomic structures of ZnO and Zn(Mg)O.³⁵ The polarization discontinuity results in a bound interface charge, which gives rise to an electric field inside the whole structure. The resulting electric field then confines free carriers close to the interface producing the 2DEG. This mechanism is akin to the proposed 2DEG confinement at polar interfaces created by ferroelectrics.^{36,37}

In this paper, we use first-principles calculations based on hybrid Hartree-Fock (HF) and DFT calculations to elucidate the origin and properties of 2DEG at the interfaces of wurtzite ZnO/Zn(Mg)O heterostructures. We calculate the charge distribution, band profile, and band alignment in the heterostructure to test that the interface charge and the electric fields in the slabs are consistent with the polarization discontinuity hypothesis. We then simulate charge doping by introducing additional n - and p -type carriers in the structure. We investigate the formation and the properties of both two-dimensional electron and hole gas (2DEG and 2DHG) at the ZnO/Zn(Mg)O interfaces.

II. METHODS AND STRUCTURE

To study the electronic structure of ZnO/Zn(Mg)O heterostructures, we use first-principles calculations based on a hybrid HF-DFT functional in a plane-wave pseudopotential approach as implemented in the Vienna *Ab initio* Simulation Package (VASP).³⁸ It is well-established that semilocal DFT functionals, such as the local density approximation (LDA) or the generalized gradient approximation (GGA), underestimate the band gap of ZnO (e.g. $E_g^{\text{GGA}} = 0.7$ eV, $E_g^{\text{Exp}} = 3.4$ eV),³⁹ resulting in incorrect band alignment in the ZnO/Zn(Mg)O heterostructures. To compensate for this deficiency, we use the Heyd-Scuseria-Ernzerhof (HSE) hybrid functional with a screening parameter of 0.2 \AA^{-1} and a nonlocal Fock-exchange parameter of 0.375, which was previously shown to correctly reproduce the electronic properties of ZnO ($E_g^{\text{HSE}} = 3.44$ eV).³⁹⁻⁴¹ For the DFT part of the calculation, we use the Perdew-Burke-Ernzerhof (PBE) exchange correlation functional.⁴² Atomic structure optimization is performed within DFT until the Hellmann-Feynman forces on each atom became less than 1.0 meV/\AA . Using the DFT calculations as a starting point, hybrid HSE calculations of the charge distribution were performed with $6 \times 6 \times 1$ Monkhorst-Pack \mathbf{k} -point grid and an energy cutoff of 500 eV for the plane wave expansion. The ion-clamped static dielectric constant is calculated in VASP as the response of the system to a small electric field $\epsilon_{ij}^\infty = \delta_{ij} + \partial P_i / \partial E_j$, where the field is 0.01 eV/\AA .

In terms of atomic structure, the binary oxides ZnO and MgO, although chemically very similar, have different structural ground states: ZnO favors a wurtzite (B4) crystal structure, while MgO prefers a rocksalt (B1) crystal structure (although the B4 structure is close in energy).³³ As a result, the ternary alloy $\text{Zn}_{1-x}\text{Mg}_x\text{O}$ exhibits a sensitive structure-composition dependence, adopting the wurtzite (B4) form only for low Mg concentrations ($x < 0.33$).⁴³⁻⁴⁵ Nevertheless, metastable structures of wurtzite Zn(Mg)O with very high Mg concentration can be achieved by epitaxial growth on high-quality ZnO crystals. This way, samples with Mg concentrations as high as 60% or more have been demonstrated.²⁸

Electronically, the Mg concentration serves to tune the Zn(Mg)O band gap gradually between that of wurtzite ZnO and MgO.^{33,43-45} The band gap of $\text{Zn}_{1-x}\text{Mg}_x\text{O}$ for a given x can be estimated from the Vegard's law $E_g^{\text{Zn(Mg)O}} = (1-x)E_g^{\text{ZnO}} + xE_g^{\text{MgO}} - bx(x-1)$, where the bowing coefficient b describes deviations from linearity.³³ Experimentally, at low concentrations, the band gap increases fairly linearly with Mg concentration.⁴³⁻⁴⁵ For higher concentrations, the bowing for the zincblende Zn(Mg)O mixture has been estimated from first-principles calculations to be moderately large, i.e. the band gap increases faster than linear with the Mg concentration.³³ Because the computational treatment of the Zn(Mg)O mixture is very challenging, we can make the calculation feasible by taking the limiting case of high-Mg concentration ($x = 1$). This simplification has the effect of somewhat exaggerating the band offset and the polarization discontinuity; however, the essential physics of the problem is preserved.

The optimized lattice parameters of the wurtzite ZnO crystal structure are $a = 3.290 \text{ \AA}$, $c/a = 1.614$, $u = 0.379$.

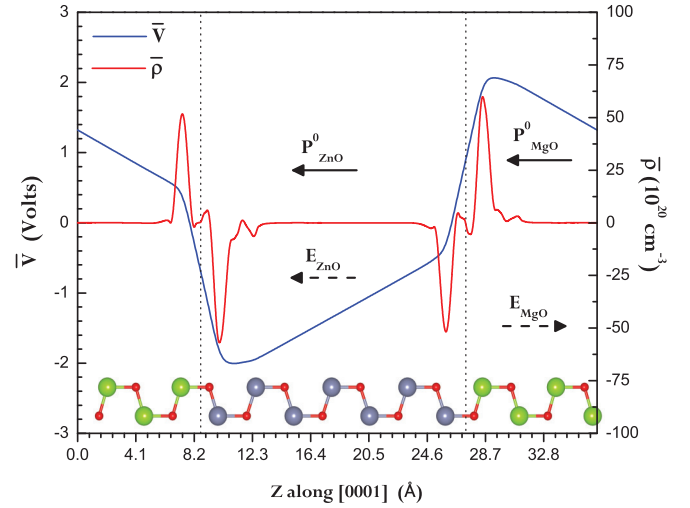


FIG. 1. (Color online) Plane-averaged total charge density $\bar{\rho}(z)$ (red line) and electrostatic potential profile $\bar{V}(z)$ along the [0001] direction in the $(\text{ZnO})_7/(\text{MgO})_7$ heterostructure. The charge density contains both the electronic and ionic charge. The zero-field polarization and electric field directions are indicated by arrows.

We constrain the in-plane lattice constant of the ZnO/MgO heterostructures to the lattice constant of ZnO in order to simulate epitaxial growth on a ZnO substrate. The theoretical lattice constant overestimates the experimental value of $a = 3.25 \text{ \AA}$; however, using the theoretical values prevents any unphysical strain. At this value of the in-plane lattice constant, the optimized wurtzite MgO structure parameters are $c/a = 1.564$, $u = 0.389$. The wurtzite $(\text{ZnO})_7/(\text{MgO})_7$ [0001] heterostructure used in the calculations is shown in Fig. 1. The ZnO wurtzite structure supports two different interfaces, Zn terminated in the positive [0001] direction and O terminated in the negative [000 $\bar{1}$] direction. Due to the periodic boundary conditions, both occur in the heterostructure. Experimentally, either one or the other can be selected by appropriate choice of the substrate.

Due to the lack of inversion symmetry, bulk ZnO exhibits spontaneous polarization in the [0001] direction (nonzero macroscopic polarization in the absence of electric fields or strain). Strain induces additional piezoelectric polarization.⁴⁶ The sum of the spontaneous and piezoelectric polarization is known as the zero-field polarization $P^0 = P^S + P^{PE}$. This polarization can be calculated from first-principles using the Berry phase method.⁴⁷ Due to its different atomic structure, Zn(Mg)O has a different value of P^0 , which changes gradually with the Mg concentration and the strain.³⁵ In addition, in ZnO/Zn(Mg)O [0001] heterostructures, there exists a discontinuity in the perpendicular component of the zero-field polarizations. Due to this discontinuity uncompensated bound charge appears at the interfaces ($\sigma_0 = P_{\text{ZnO}}^0 - P_{\text{ZnMgO}}^0$). This bound charge produces a depolarizing electric field which tends to soften the polarization discontinuity. Since the depolarizing field depends on the sample geometry and boundary conditions, the total interface charge and, respectively, the electric field inside the slab cannot be determined from the zero-field polarization alone.

III. RESULTS AND DISCUSSION

A. Macroscopic total charge density and potential profiles

We perform first-principles calculations of the electronic structure of the wurtzite ZnO/MgO [0001] heterostructure. We first converge the charge density and wave functions in a DFT calculation, which are used as the starting point for the HSE calculation. Then the total electrostatic potential, including the electronic and ionic contributions, is calculated within HSE. The xy -averaged macroscopic charge density is obtained from the averaged potential as $\bar{\rho}(z) = -\frac{\epsilon_0 \partial^2 \bar{V}(z)}{\partial z^2}$. It contains the contributions from valence and core electrons as well as ions. In Fig. 1, the xy -averaged macroscopic charge density $\bar{\rho}(z)$ and potential profile $\bar{V}(z)$ are shown along the [0001] direction. It can be seen from the figure that the total charge density is nonzero only near the interfaces where dipoles are present. The charge density dipoles correspond to the electronic response to the formation of the interface.⁴⁸ What is particular to the ZnO/MgO interface is that the dipole is not symmetric, indicating the accumulation of net charge at the interface. Integration of the charge density around the [0001] interface gives a net surface charge of -1.264×10^{13} e/cm² and exactly the same amount of positive charge at the [000 $\bar{1}$] interface. Correspondingly, we find that the potential exhibits large jumps close to the interfaces due to the interface dipoles, but it is linear inside the bulk of the ZnO and MgO. This indicates a lack of charge and a constant electric field in the bulk of the slabs. We estimate the electric fields in both slabs from the slope of the potential to be $E_{\text{ZnO}} = -1.13 \times 10^9$ V/m and $E_{\text{MgO}} = -1.15 \times 10^9$ V/m, respectively.

Next, we check if the obtained electrostatic potential profile in the heterostructure is consistent with polarization discontinuity. In experiment, the interface is formed between two thick slabs of ZnO and Zn(Mg)O in contact with the environment (substrate, capping layer, or free surface). Thus, boundary conditions will have a significant effect on the electrostatic profile in the heterostructure. We model it by a heterojunction made of materials 1 and 2 with lengths l_1 and l_2 ($L = l_1 + l_2$), and dielectric constants ϵ_1 and ϵ_2 , respectively. Free charges from the environment will accumulate at the outside surfaces. The accumulated charge would be sufficient to make the electric field outside the sample vanish. Under this condition, we find that the net effect of the boundary conditions can be summarized by a potential ΔV across the heterojunction or equivalently a net electric field $E_{\text{net}} = \Delta V/L$ (for derivation details, see the Appendix). In terms of E_{net} , the polarization screened surface charge density σ' and the electric fields inside materials 1 and 2 can be expressed as

$$\begin{aligned} \sigma' &= -\frac{\Delta P^0}{\bar{\epsilon}'} + \frac{\Delta \epsilon}{\bar{\epsilon}'} \frac{\Delta V}{L}, \\ E_1 &= -\frac{\Delta P^0}{\bar{\epsilon}} \left(\frac{l_2}{L} \right) + \frac{\epsilon_2}{\bar{\epsilon}} \frac{\Delta V}{L}, \\ E_2 &= \frac{\Delta P^0}{\bar{\epsilon}} \left(\frac{l_1}{L} \right) + \frac{\epsilon_1}{\bar{\epsilon}} \frac{\Delta V}{L}, \end{aligned} \quad (1)$$

where $\Delta \epsilon = \epsilon_1 - \epsilon_2$ is the dielectric constant discontinuity, $\Delta P^0 = P_1^0 - P_2^0$ is the zero-field polarization discontinuity, $\bar{\epsilon} = (l_2/L)\epsilon_1 + (l_1/L)\epsilon_2$, and $\bar{\epsilon}' = \frac{\bar{\epsilon}}{\epsilon_0}$.

TABLE I. Zero-field polarization and electronic dielectric constant of bulk wurtzite ZnO and MgO, with the surface charge and electric fields predicted from the polarization discontinuity model. The values obtained in the direct heterostructure calculation are given in brackets.

	P^0 (C/m ²)	ϵ/ϵ_0	σ ($\times 10^{13}$ cm ⁻²)	E ($\times 10^9$ V/m)
ZnO	-0.030	3.434	1.268 (1.264)	-1.12 (-1.13)
MgO	-0.089	2.652	-1.268 (-1.264)	1.17 (1.15)

In our calculation, the use of the short-circuit boundary condition that net electric field in the heterostructure vanishes, $E_{\text{net}} = 0$. In the first principles calculation, this condition is enforced by the periodic boundary conditions. Under this condition, the bound charge and the electric fields in the slabs are given by

$$\sigma' = -\frac{\Delta P^0}{\bar{\epsilon}'}; \quad E_1 = -\frac{\Delta P^0}{\bar{\epsilon}} \left(\frac{l_2}{L} \right); \quad E_2 = \frac{\Delta P^0}{\bar{\epsilon}} \left(\frac{l_1}{L} \right), \quad (2)$$

which means that the polarization discontinuity largely determines the bound charge at the interface. While the electric fields in the slabs depend on the bound charge and the relative slab thicknesses. More general boundary conditions, in principle, can be also modeled by the application of electric field. A net electric field would skew the potential profile but would not change the key feature, namely the presence of a confining potential at the interface, and therefore the physics of the 2DEG formation (for a discussion see the Appendix).

Now we set out to calculate the theoretically predicted bound charge and electric fields. First, Berry phase calculations of the polarization in bulk wurtzite ZnO and MgO are performed with in HSE resulting in $P_{\text{ZnO}}^0 = -0.030$ C/m² and $P_{\text{Zn(Mg)O}}^0 = -0.089$ C/m² (Table I). Both materials have the ZnO theoretical lattice constant in the plane, which means that the polarization values reflect the spontaneous polarization of ZnO and the spontaneous plus piezoelectric polarization of MgO. In the case of Zn_{1-x}Mg_xO the spontaneous polarization is a function of the Mg content.³⁵ Thus, experimentally, the polarization discontinuity would be less than in our calculations performed with $x = 1$. Furthermore, we calculate the dielectric constant in both materials (Table I). In practice, the polarization charge is screened by both electrons and ions.⁴⁹ In order to simplify the calculations, however, we take the ions to be clamped, which corresponds to using the ion-clamped instead of the full static dielectric constant.

We use the calculated values of the zero-field polarization and the dielectric constant to calculate the induced charge at the interfaces σ and the electric field E in both slabs using Eq. (2). The theoretical values are given in Table I together with the values from the heterostructure calculations obtained earlier (in brackets). We find an excellent agreement between the model values and the values obtained by direct computation, which indicates that the accumulated charge at the interface and the electric fields are consistent with the polarization discontinuity hypothesis.

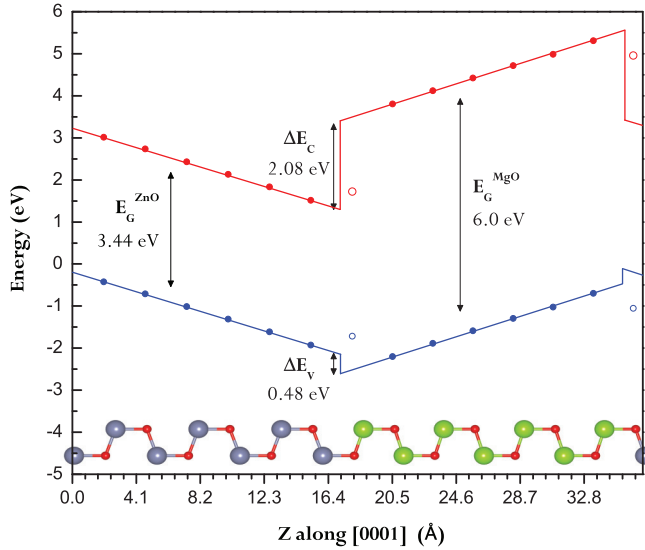


FIG. 2. (Color online) Valence band maximum (blue) and conduction band minimum (red) profile along the [0001] direction in the $(\text{ZnO})_7/(\text{MgO})_7$ heterostructure. Blue and red circles indicate the positions of the VBM and CBM, respectively. Empty circles indicate the band edges derived from the interface O. The lines are an interpolation.

B. Valence band maximum (VBM) and conduction band minimum (CBM) profiles

The confinement mechanism of the 2DEG can be understood by the band profile in the ZnO/MgO heterostructure. The band profile is a result of the interplay between the electric field in the slabs, the potential jumps at the interfaces, and the bulk band gaps of the two materials. For that purpose, we trace the corelike O-2s localized a distance $\Delta\varepsilon_{VBM} = 18.13$ eV below the VBM in bulk ZnO. Since they do not participate in bonding, their shifts are caused entirely by the local electrostatic potential.¹⁷ In terms of the O-2s band center ε_l on each layer l , the VBM and CBM are given

$$\text{VBM}_l = \varepsilon_l + \Delta\varepsilon_{VBM}; \quad \text{CBM}_l = \text{VBM}_l + E_g, \quad (3)$$

where E_g is the band gap of ZnO (MgO). The valence band of ZnO is composed of filled O-2p and Zn-3d bands, while the conduction band has predominantly Zn-4s character. Within HSE, the ZnO band gap is calculated to be $E_g^{\text{ZnO}} = 3.44$ eV. Similarly, the valence band of the MgO consists of O-2p orbitals, and the conduction band consists of Mg-3s orbitals. The HSE band gap of wurtzite MgO is $E_g^{\text{MgO}} = 6.0$ eV. Although there is no experimental data for the band gap of wurtzite MgO, HSE predicts the band gap of rocksalt MgO to be $E_g^{\text{MgO}} = 7.37$ eV, which is in good agreement with experiment ($E_g^{\text{MgO,Exp}} = 7.67$ eV).³³ Doping of ZnO with Mg smoothly interpolates the band gap of the alloy between these values.

The resulting ZnO/MgO band profile and band offsets are shown in Fig. 2. The CBM and VBM profiles portray a straddling gap (type I) heterostructure. The valence band offset is small ($\Delta E_v = 0.48$ eV) due to the common anion. The conduction band offset is relatively large ($\Delta E_c = 2.08$ eV) and can be controlled through the amount of Mg doping. We find

that the band profiles are linear and consistent with the electric field in the two slabs, except very close to the interface where the interface dipole is felt. The combination of electric field and band offsets create a wedge-shaped potential well which can confine free electrons at the [0001] interface and holes in the $[000\bar{1}]$ interface.

We note that, in our calculation, there are no free charges and therefore no band bending. Given the constant electric field, increasing the size of the slab would increase the potential until band overlap occurs, i.e. the VBM is above the CBM, and the heterostructure no longer has a gap. This condition sets practical limits to the size of the supercell we can use. In the experimental setup, due to the electric field in the slabs, the free charges will be transferred from the surfaces to the interface until the electric field far from the interface is completely screened. This will produce band bending close to the interface. To simulate this process, we need to add extra carriers to the structure.

C. 2DEG and 2DHG charge density profile

In order to investigate how the charge is localized close to the interfaces, we add n - or p -type carriers to the $(\text{ZnO})_7/(\text{ZnMgO})_7$ heterostructure. To keep the system charge neutral, the extra valence charge is compensated by a uniform background charge of the opposite sign. In order to simulate n -type/ p -type carriers, we add/remove a total charge $0.001e$ per supercell corresponding to a surface charge density of 1×10^{12} e/cm², which is in the lower end of experimental concentrations.^{25,27} The resulting charge distribution of the free carriers is obtained by summing the partial charge density of all occupied conduction band states (n -type) or all empty valence band states (p -type), $\sum_{n,k} |\phi_{nk}|^2$, where the sum is over the corresponding bands and k -points in the Brillouin zone.

The resulting carrier distributions are shown in Figs. 3(a) and 3(b) for n - and p -type doping, respectively. We see that electrons are confined by the triangular potential at the [0001] interface. Most of the charge is on the ZnO side (with some spilling in the MgO), and the whole charge is confined within 2 nm from the interface. The effective mass of the electrons in the 2DEG is $m_e^* = 0.20m_e$, as calculated from a quadratic interpolation of the ZnO conduction band in the plane parallel to the interface. This value is in good agreement with experiment^{25,50} and is about two orders of magnitude smaller than that in the $\text{LaAlO}_3/\text{SrTiO}_3$ case.¹⁷

In the case of hole doping, the carriers are confined at the $[000\bar{1}]$ interface. The confinement width is even smaller, of the order of 1 nm, which is consistent with the more localized nature of the O- p states. The effective hole mass is calculated to be $m_h^* = 1.85m_e$. Experimentally, only a 2DEG has been observed, possibly because the native point defects in ZnO lead to unintentional n -type conductivity. At the same time, it has been very challenging to achieve p -type conductivity in ZnO.⁵¹ Another consideration is the possible formation of O vacancies which trap the holes.^{52,53} A similar 2DHG was predicted at Al-terminated $\text{LaAlO}_3/\text{SrTiO}_3$ interfaces¹¹ but was never observed experimentally, very likely due to the formation of O vacancies.

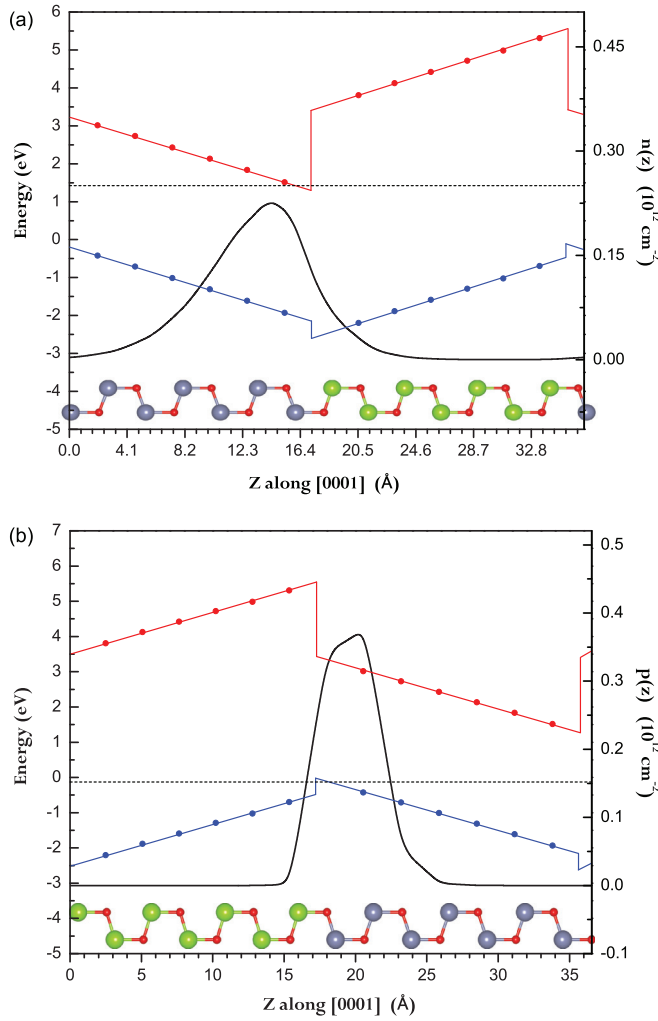


FIG. 3. (Color online) Charge density distribution of the two-dimensional gas in (a) n -type and (b) p -type doped $(\text{ZnO})_7/(\text{ZnMgO})_7$ heterostructure. Here, the 2DEG forms at the $[0001]$ interface and the 2DHG forms at the $[000\bar{1}]$ interface. The Fermi energy is indicated by the dashed line. The undoped band profile is shown as a reference.

Thus, indeed, we find that a large amount of charge, both n and p type, can be confined very close to the interface. In practice, the amount of charge transferred from the surfaces would be enough to completely screen the electric field, i.e. equal to the bound charge σ . Thus, the surface charge density of the 2DEG can be directly controlled through the amount of Mg doping [Eq. (1)]. Moreover, the confinement width can be tuned by the sample slab dimensions [Eq. (2)].

IV. CONCLUSIONS

We have performed first-principles hybrid HF-DFT calculations of the band alignment and charge distribution in wurtzite $\text{ZnO}/\text{Zn}(\text{Mg})\text{O}$ $[0001]$ heterostructures. We show that the potential profile is consistent with the hypothesis of polarization discontinuity at the interface between the two materials. We demonstrate that both n - and p -type carriers can be confined at the interfaces. The type of carriers in the gas, 2DEG or 2DHG, can be controlled by choosing the interface termination, and the charge density can be tuned by the amount of Mg doping.

We find that the charge channel is very narrow, on the order of 1 nm, which is comparable with other oxide 2DEGs, but the charge mobility is expected to be significantly higher due to the lower effective mass of the carriers. The confinement width may also be controlled through the device dimensions. We expect that the practical implementation of a 2DHG would be hampered by O vacancies in the ZnO, a problem which would require further investigation. Overall, our results suggest that $\text{ZnO}/\text{Zn}(\text{Mg})\text{O}$ heterostructures combine the advantages of both semiconducting and oxide materials, displaying high carrier mobility, strong confinement, and a high level of tunability. This could make them excellent candidates for novel electronics applications.

ACKNOWLEDGMENTS

This work was supported by the National Science Foundation through Nebraska and Puerto-Rico EPSCOR (Grants Nos. EPS-1010674, EPS-1002410 and EPS-1010094), Nebraska MRSEC (Grant No. DMR-0820521) and DMR (Grant No. DMR-1105474), and the Department of Energy (Grant No. DE-FG02-08ER46526). Computations were performed at the Holland Computing Center at the University of Nebraska-Lincoln.

APPENDIX

Here, we discuss in detail the electrostatic boundary conditions of the problem. The model geometry is illustrated in Fig. 4(a). The interface is formed between two thick slabs of ZnO and $\text{Zn}(\text{Mg})\text{O}$ of lengths l_1 and l_2 and dielectric constants ϵ_1 and ϵ_2 , respectively. The two slabs have zero-field polarizations P_1^0 and P_2^0 . The polarization discontinuity ($P_2^0 > P_1^0$) creates bound charges at the surfaces and at the interface. The amount of charge and the electric fields in the slabs, however, will depend on the boundary conditions.

In the case of a linear dielectric, the induced polarization is proportional to the applied electric field $P = \epsilon_0 \chi E$, where χ is the dielectric susceptibility. Then the electric displacement is $D = \epsilon E$, where $\epsilon = \epsilon_0 \epsilon'$ is the permittivity of the material and $\epsilon' = 1 + \chi$ is the relative permittivity or dielectric constant of the material. The Gauss law then becomes $\nabla \cdot \mathbf{D} = \rho_f$, where ρ_f are the free charges (i.e. not coming from the polarization). If there are no free charges, $\nabla \cdot \mathbf{D} = 0$. In the presence of spontaneous polarization, $P = P^0 + \epsilon_0 \chi E$. In this case, it is convenient to use the same definition of the displacement $D = \epsilon E$, i.e. the displacement includes only the effect of the induced polarization, in which case the Gauss law becomes $\nabla \cdot \mathbf{D} = -\nabla \cdot \mathbf{P}^0$. In other words, the bound charges resulting from the spontaneous polarization are treated as free charges.

Let us now consider our system in vacuum. The charges resulting from the spontaneous polarization are $\sigma_1 = P_1^0$, $\sigma_2 = P_2^0$, and $\sigma_i = \sigma_1 - \sigma_2 = P_1^0 - P_2^0 = \Delta P^0$, as indicated in Fig. 4. Using that the displacement due to a charged plane with surface charge density σ is $D = \sigma/2$, we find for the field outside of the sample $D_{\text{out}} = (-\sigma_1 + \sigma_2 + \sigma_i)/2 = 0$. The displacement in each of the slabs is

$$\begin{aligned} D_1 &= \frac{1}{2}(-\sigma_1 - \sigma_2 - \sigma_i) = -\sigma_1 = \epsilon_1 E_1 \\ D_2 &= \frac{1}{2}(-\sigma_1 - \sigma_2 + \sigma_i) = -\sigma_2 = \epsilon_2 E_2 \end{aligned} \quad (\text{A1})$$

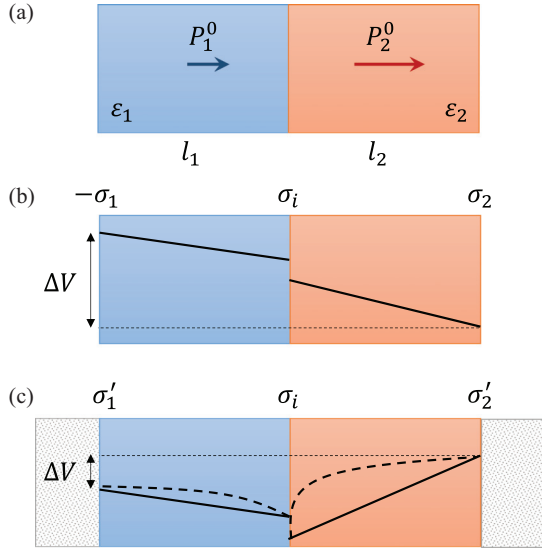


FIG. 4. (Color online) (a) Schematic view of the heterostructure between two slabs with spontaneous polarizations P_1^0 and P_2^0 , electric permittivities ϵ_1 and ϵ_2 , and lengths l_1 and l_2 . Boundary conditions and electrostatic potential profile for (b) vacuum and (c) connected to the environment.

therefore, in both slabs the electric fields are negative, $E_1 = -P_1^0/\epsilon_1$ and $E_2 = -P_2^0/\epsilon_2$. The resulting electrostatic profile is shown in Fig. 4(b), where we have taken into account the boundary condition at the interface $\epsilon_2 E_2 - \epsilon_1 E_1 = \sigma_1 - \sigma_2 = \Delta P^0$. In this case, there cannot be any accumulation of charge at the interface. The net potential drop across the sample is

$$\Delta V = E_1 l_1 + E_2 l_2 = - \left(\frac{P_1^0 l_1}{\epsilon_1} + \frac{P_2^0 l_2}{\epsilon_2} \right), \quad (\text{A2})$$

corresponding to a net electric field $E_{\text{net}} = \frac{\Delta V}{L}$, which will drive any free charges to one of the surfaces.

In practice, the system is not in vacuum. Both surfaces are in contact with the environment (substrate, capping layer, air), which serves as a reservoir for free charges. Charges will accumulate at the surfaces until the electric field out of the sample vanishes. For the sake of argument, let us assume that the charges remain at the surfaces. In that case, we label the new surface charges σ'_1 and σ'_2 . The electric displacement outside of the sample can be written as

$$D_{\text{out}} = \frac{1}{2}(\sigma'_1 + \sigma'_2 + \sigma_i) = 0, \quad (\text{A3})$$

from where it follows that $\sigma_i = -(\sigma'_1 + \sigma'_2)$, i.e. the total amount of surface charge, would exactly compensate the interface charge. This condition is satisfied in vacuum, too; however, the availability of free charges allows redistribution of the charge between the surfaces. Similarly, we can write the displacement in each of the slabs as

$$\begin{aligned} D_1 &= \frac{1}{2}(\sigma'_1 - \sigma'_2 - \sigma_i) = \sigma'_1, \\ D_2 &= \frac{1}{2}(\sigma'_1 - \sigma'_2 + \sigma_i) = -\sigma'_2, \end{aligned} \quad (\text{A4})$$

from which using that the electric field is $E_i = D_i/\epsilon_i$ and that the potential drop throughout the sample is $\Delta V = E_1 l_1 + E_2 l_2$. We can solve for the surface charges in terms of the

potential difference and the interface charge

$$\begin{aligned} \sigma'_1 &= -\sigma_i \frac{\epsilon_1 l_2}{\bar{\epsilon}} L + \frac{\epsilon_1 \epsilon_2 \Delta V}{\bar{\epsilon} L}, \\ \sigma'_2 &= -\sigma_i \frac{\epsilon_2 l_1}{\bar{\epsilon}} L - \frac{\epsilon_1 \epsilon_2 \Delta V}{\bar{\epsilon} L}, \end{aligned} \quad (\text{A5})$$

where we have defined $\bar{\epsilon} = (\epsilon_1 l_2 + \epsilon_2 l_1)/L$ and $L = l_1 + l_2$. Substituting back in the electric fields, we obtain

$$\begin{aligned} E_1 &= \frac{\sigma'_1}{\epsilon_1} = -\frac{\Delta P^0 l_2}{\bar{\epsilon} L} + \frac{\epsilon_2 \Delta V}{\bar{\epsilon} L}, \\ E_2 &= -\frac{\sigma'_2}{\epsilon_2} = \frac{\Delta P^0 l_1}{\bar{\epsilon} L} + \frac{\epsilon_1 \Delta V}{\bar{\epsilon} L}, \end{aligned} \quad (\text{A6})$$

from which we immediately see that there are two contributions to the field: from the polarization discontinuity and from the external potential. The contribution from the polarization is opposite in the two slabs, producing the confining potential as illustrated in Fig. 4(c) (solid line). The effect of the external potential is to add a net electric field the effect, which is to tilt the polarization fields in the same direction.

We can also estimate the total interface charge accounting for the polarization of the dielectric as

$$\sigma'_i = \epsilon_0(E_1 - E_2) = -\frac{\Delta P^0}{\bar{\epsilon}'} + \frac{\Delta \epsilon \Delta V}{\bar{\epsilon}' L}, \quad (\text{A7})$$

where $\Delta \epsilon = \epsilon_1 - \epsilon_2$ and $\bar{\epsilon}' = \frac{\bar{\epsilon}}{\epsilon_0}$. Here, also, there are two contributions: the polarization discontinuity and the external potential. However, if the dielectric constants of the two materials are similar, the effect of the external potential would be minimal, so we can conclude that the polarization discontinuity essentially determines the interfacial charge.

If the amount of interface charge is weakly dependent on the boundary conditions (ΔV) and the sample geometry (l_1 and l_2), the amount of screening charge at the surfaces and the electric field in the slabs depends strongly on the boundary conditions. Quite possibly, different boundary conditions are realized in the different experiments. We saw, however, that all these support a confining potential, the effect of the boundary condition being an overall tilt of the potential profile. From first principles, these different conditions can be simulated by adding an overall electric field in the structure. However, the simplest condition of no electric field ($\Delta V = 0$) already displays the essential physics of the problem. In our calculations, the periodic boundary conditions without an external electric field realize the $\Delta V = 0$ boundary condition. Experimentally, this also corresponds to the most probable case of a short-circuit boundary condition. When the environment is leaky due to the potential difference, charges will be transferred from the surface with the higher potential to that with the lower until $\Delta V = 0$. In this case, the electric fields will be

$$E_1 = -\frac{\Delta P^0 l_2}{\bar{\epsilon} L}; \quad E_2 = \frac{\Delta P^0 l_1}{\bar{\epsilon} L}, \quad (\text{A8})$$

and the polarization screened interface charge is

$$\sigma'_i = -\frac{\Delta P^0}{\bar{\epsilon}'}. \quad (\text{A9})$$

Finally, in experiment, the strong electric field in the slabs will drive charge into the system and will be distributed close to the interface in accordance with the Poisson law. Thus, the net charge away from the interface will be zero, and the electric field outside of the sample and inside the

slabs far from the interface will be zero, i.e. $E_1 = E_2 = 0$. This will produce band bending close to the interface, and the potential will tend to a constant in the slabs sufficiently far from the interface as illustrated in Fig. 4(c) (dashed line).

- ¹A. P. Ramirez, *Science* **315**, 1377 (2007).
- ²J. Mannhart and D. G. Schlom, *Science* **327**, 1607 (2010).
- ³P. Zubko, S. Gariglio, M. Gabay, P. Ghosez, and J.-M. Triscone, *Ann. Rev. Cond. Matt. Phys.* **2**, 141 (2011).
- ⁴J. Chakhalian, A. J. Millis, and J. Rondinelli, *Nat. Mater.* **11**, 92 (2012).
- ⁵H. Y. Hwang, Y. Iwasa, M. Kawasaki, B. Keimer, N. Nagaosa, and Y. Tokura, *Nat. Mater.* **11**, 103 (2012).
- ⁶A. Ohtomo, D. A. Muller, J. L. Grazul, and H. Y. Hwang, *Nature* **419**, 378 (2002).
- ⁷A. Ohtomo and H. Y. Hwang, *Nature* **427**, 423 (2004).
- ⁸S. Thiel, G. Hammerl, A. Schmehl, C. W. Schneider, and J. Mannhart, *Science* **313**, 1942 (2006).
- ⁹N. Nakagawa, H. Y. Hwang, and D. A. Muller, *Nat. Mater.* **5**, 204 (2006).
- ¹⁰S. Okamoto, A. J. Millis, and N. A. Spaldin, *Phys. Rev. Lett.* **97**, 056802 (2006).
- ¹¹M. S. Park, S. H. Rhim, and A. J. Freeman, *Phys. Rev. B* **74**, 205416 (2006).
- ¹²J. Lee and A. A. Demkov, *Phys. Rev. B* **78**, 193104 (2008).
- ¹³Z. S. Popovic, S. Satpathy, and R. M. Martin, *Phys. Rev. Lett.* **101**, 256801 (2008).
- ¹⁴K. Janicka, J. P. Velev, and E. Y. Tsymbal, *J. Appl. Phys.* **103**, 07B508 (2008).
- ¹⁵M. Huijben, A. Brinkman, G. Koster, G. Rijnders, H. Hilgenkamp, and D. H. A. Blank, *Adv. Mater.* **21**, 1665 (2009).
- ¹⁶R. Pentcheva and W. E. Pickett, *Phys. Rev. Lett.* **102**, 107602 (2009).
- ¹⁷K. Janicka, J. P. Velev, and E. Y. Tsymbal, *Phys. Rev. Lett.* **102**, 106803 (2009).
- ¹⁸H. Chen, A. M. Kolpak, and S. Ismail-Beigi, *Adv. Mater.* **22**, 2881 (2010).
- ¹⁹H. W. Jang, D. A. Felker, C. W. Bark, Y. Wang, M. K. Niranjan, C. T. Nelson, Y. Zhang, D. Su, C. M. Folkman, S. H. Baek, S. Lee, K. Janicka, Y. Zhu, X. Q. Pan, D. D. Fong, E. Y. Tsymbal, M. S. Rzchowski, and C. B. Eom, *Science* **331**, 886 (2011).
- ²⁰B. R. K. Nanda and S. Satpathy, *Phys. Rev. Lett.* **101**, 127201 (2008).
- ²¹P. Moetakef, T. A. Cain, D. G. Ouellette, J. Y. Zhang, D. O. Klenov, A. Janotti, C. G. Van de Walle, S. Rajan, S. J. Allen, and S. Stemmer, *Appl. Phys. Lett.* **99**, 232116 (2011).
- ²²Y. Wang, M. K. Niranjan, J. D. Burton, J. M. An, K. D. Belashchenko, and E. Y. Tsymbal, *Phys. Rev. B* **79**, 212408 (2009).
- ²³J. D. Burton and E. Y. Tsymbal, *Phys. Rev. Lett.* **107**, 166601 (2011).
- ²⁴H. Tampo, H. Shibata, K. Matsubara, A. Yamada, P. Fons, S. Niki, M. Yamagata, and H. Kanie, *Appl. Phys. Lett.* **89**, 132113 (2006).
- ²⁵A. Tsukazaki, A. Ohtomo, T. Kita, Y. Ohno, H. Ohno, and M. Kawasaki, *Science* **315**, 1388 (2007).
- ²⁶A. Tsukazaki, H. Yuji, S. Akasaka, K. Tamura, K. Nakahara, T. Tanabe, H. Takasu, A. Ohtomo, and M. Kawasaki, *Appl. Phys. Express* **1**, 055004 (2008).
- ²⁷H. Tampo, H. Shibata, K. Maejima, A. Yamada, K. Matsubara, P. Fons, S. Kashiwaya, S. Niki, Y. Chiba, T. Wakamatsu, and H. Kanie, *Appl. Phys. Lett.* **93**, 202104 (2008).
- ²⁸H. Tampo, H. Shibata, K. Maejima, T.-W. Chiu, H. Itoh, A. Yamada, K. Matsubara, P. Fons, Y. Chiba, T. Wakamatsu, Y. Takeshita, H. Kanie, and S. Niki, *Appl. Phys. Lett.* **94**, 242107 (2009).
- ²⁹A. Tsukazaki, S. Akasaka, K. Nakahara, Y. Ohno, H. Ohno, D. Maryenko, A. Ohtomo, and M. Kawasaki, *Nat. Mater.* **9**, 889 (2010).
- ³⁰H. Chen, S. Gu, J. Liu, J. Ye, K. Tang, S. Zhu, and Y. Zheng, *Appl. Phys. Lett.* **99**, 211906 (2011).
- ³¹J. Ye, S. T. Lim, M. Bosman, S. Gu, Y. Zheng, H. H. Tan, C. Jagadish, X. Sun, and K. L. Teo, *Sci. Rep.* **2**, 533 (2012).
- ³²K. Han, N. Tang, J. D. Ye, J. X. Duan, Y. C. Liu, K. L. Teo, and B. Shen, *Appl. Phys. Lett.* **100**, 192105 (2012).
- ³³Y. Z. Zhu, G. D. Chen, and H. Ye, A. Walsh, C. Y. Moon, and S.-H. Wei, *Phys. Rev. B* **77**, 245209 (2008).
- ³⁴T. Dietl, H. Ohno, F. Matsukura, J. Cibert, and D. Ferrand, *Science* **287**, 1019 (2000).
- ³⁵A. Malashevich and D. Vanderbilt, *Phys. Rev. B* **75**, 045106 (2007).
- ³⁶M. K. Niranjan, Y. Wang, S. S. Jaswal, and E. Y. Tsymbal, *Phys. Rev. Lett.* **103**, 016804 (2009).
- ³⁷Y. Wang, M. K. Niranjan, K. Janicka, J. P. Velev, M. Y. Zhuravlev, S. S. Jaswal, and E. Y. Tsymbal, *Phys. Rev. B* **82**, 094114 (2010).
- ³⁸G. Kresse and J. Furthmüller, *Phys. Rev. B* **54**, 11169 (1996).
- ³⁹J. Heyd, G. E. Scuseria, and M. Ernzerhof, *J. Chem. Phys.* **118**, 8207 (2003).
- ⁴⁰F. Oba, A. Togo, I. Tanaka, J. Paier, and G. Kresse, *Phys. Rev. B* **77**, 245202 (2008).
- ⁴¹J. Wróbel, K. J. Kurzydłowski, K. Hummer, G. Kresse, and J. Piechota, *Phys. Rev. B* **80**, 155124 (2009).
- ⁴²J. P. Perdew, K. Burke, and M. Ernzerhof, *Phys. Rev. Lett.* **77**, 3865 (1996).
- ⁴³A. Ohtomo, M. Kawasaki, T. Koida, K. Masubuchi, H. Koinuma, Y. Sakurai, Y. Yoshida, T. Yasuda, and Y. Segawa, *Appl. Phys. Lett.* **72**, 2466 (1998).
- ⁴⁴T. Makino, Y. Segawa, M. Kawasaki, A. Ohtomo, R. Shiroki, K. Tamura, T. Yasuda, and H. Koinuma, *Appl. Phys. Lett.* **78**, 1237 (2001).
- ⁴⁵A. Singh, A. Vij, D. Kumar, P. K. Khanna, M. Kumar, S. Gautam, and K. H. Chae, *Semicond. Sci. Technol.* **28**, 025004 (2013).
- ⁴⁶C. W. Bark, D. A. Felker, Y. Wang, Y. Zhang, H. W. Jang, C. M. Folkman, J. W. Park, S. H. Baek, X. Q. Pan, E. Y. Tsymbal, M. S. Rzchowski, and C. B. Eom, *Proc. Natl. Acad. Sci.* **108**, 4720 (2011).
- ⁴⁷A. Dal Corso, M. Posternak, R. Resta, and A. Baldereschi, *Phys. Rev. B* **50**, 10715 (1994).
- ⁴⁸F. Bernardini and V. Fiorentini, *Phys. Rev. B* **57**, 9427 (1998).

- ⁴⁹G. Gerra, A. K. Tagantsev, N. Setter, and K. Parlinski, *Phys. Rev. Lett.* **96**, 107603 (2006).
- ⁵⁰A. Tsukazaki, A. Ohtomo, M. Kawasaki, S. Akasaka, H. Yuji, K. Tamura, K. Nakahara, T. Tanabe, A. Kamisawa, T. Gokmen, J. Shabani, and M. Shayegan, *Phys. Rev. B* **78**, 233308 (2008).
- ⁵¹A. Janotti and C. G. Van de Walle, *Rep. Prog. Phys.* **72**, 126501 (2009).
- ⁵²Z. Zhong, P. X. Xu, and P. J. Kelly, *Phys. Rev. B* **82**, 165127 (2010).
- ⁵³L. Zhang, X.-F. Zhou, H.-T. Wang, J.-J. Xu, J. Li, E. G. Wang, and S.-H. Wei, *Phys. Rev. B* **82**, 125412 (2010).